Bioorthogonal Reactions

Deutsche Ausgabe: DOI: 10.1002/ange.201608504
Internationale Ausgabe: DOI: 10.1002/anie.201608504

Cathepsin B-Specific Metabolic Precursor for In Vivo Tumor-Specific Fluorescence Imaging

*Man Kyu Shim[+], Hong Yeol Yoon[+], Ju Hee Ryu, Heebeom Koo, Sangmin Lee, Jae Hyung Park, Jong-Ho Kim, Seulki Lee, Martin G. Pomper, Ick Chan Kwon, and Kwangmeyung Kim**

Abstract: *Recently, metabolic glycoengineering with bioorthogonal click reactions has focused on improving the tumor targeting efficiency of nanoparticles as delivery vehicles for anticancer drugs or imaging agents. It is the key technique for developing tumor-specific metabolic precursors that can generate unnatural glycans on the tumor-cell surface. A cathepsin B-specific cleavable substrate (KGRR) conjugated with triacetylated N-azidoacetyl-D-mannosamine (RR-S-Ac_3ManNAz) was developed to enable tumor cells to generate unnatural glycans that contain azide groups. The generation of azide groups on the tumor cell surface was exogenously and specifically controlled by the amount of RR-S-Ac_3ManNAz that was fed to target tumor cells. Moreover, unnatural glycans on the tumor cell surface were conjugated with near infrared fluorescence (NIRF) dye-labeled molecules by a bioorthogonal click reaction in cell cultures and in tumor-bearing mice. Therefore, our RR-S-Ac_3ManNAz is promising for research in tumor-specific imaging or drug delivery.*

Metabolic glycoengineering is a useful biological technique, which utilizes the intrinsic glycan metabolism of cells to introduce unnatural glycans with various chemical groups such as ketones, thiols, alkynes, azides, and bicyclononynes.[1] When the cells are treated with unnatural metabolic precursors, they use them as building blocks for glycan metabolism and these precursors containing azide groups ($-N_3$) are exogenously generated on the cell surface.[2] Particularly, bioorthogonal click molecules could be chemically bound to the unnatural glycans by click chemistry in living cells or organisms as well as ex vivo conditions for various biomedical applications.[3]

Recently, we have also focused on the use of bioorthogonal click chemistry in new active-targeting strategies for tumor-targeted nanoparticles for delivering imaging agents or anticancer drugs. The active-targeting efficiency of nanoparticles is still limited and there are many obstacles to improving their tumor-targeting efficacy in vivo.[4] Until now, nanoparticle surfaces have been extensively modified with tumor-targeted biological ligands such as antibodies, peptides, aptamers, and glucoses, which can specifically bind to the overexpressed biological receptors.[5] However, the expression level of biological receptors on tumor cells has been reported to be usually saturated and insufficient for nanoparticle targeting.[4] To surmount the lower tumor-targeting efficiency of the traditional active-targeting strategy, we have suggested the use of exogenous chemical receptors that can be produced on the tumor-cell surface by using metabolic glycoengineering.[6] The intra-tumorally-injected metabolic precursors could produce the unnatural glycans containing azide groups ($-N_3$) on the tumor cells by metabolic glycoengineering. Subsequently, the chemical receptors of unnatural glycans could be successfully targeted using bioorthogonal click-molecule-conjugated nanoparticles in tumor-bearing mice. However, the biggest drawback of metabolic glycoengineering in tumor-targeting delivery systems is that the intravenously injected metabolic precursors do not have any specificity against the targeted tumor cells in vivo, resulting in the production of the same exogenous chemical receptors on the surface of both normal cells and tumor cells.[7] Therefore, newly designed metabolic precursors with targeted tumor-cell specificity are urgently needed in tumor imaging and treatment.

Bertozzi's group recently introduced a prostate-tumor-cell-specific caged metabolic precursor with a prostate-specific antigen (PSA) protease-specific cleavable peptide substrate.[8] Although PSA protease-specific metabolic precursors showed high-specificity for the targeted prostate tumor cells in the cell culture system, this approach had potential problems for use under in vivo conditions. This is because the PSA protease-specific metabolic precursors are degraded by PSA protease in the blood and then the uncaged metabolites

[*] M. K. Shim,[+] Dr. H. Y. Yoon,[+] Dr. J. H. Ryu, Dr. S. M. Lee, Dr. I. C. Kwon, Dr. K. M. Kim
Center for Theragnosis, Biomedical Research Institute
Korea Institute of Science and Technology
5, Hwarang-ro 14-gil, Seongbuk-gu, Seoul 02792 (Republic of Korea)
E-mail: kim@kist.re.kr
Dr. H. Koo
Department of Medical Life Science, College of Medicine
The Catholic University of Korea
222, Banpo-daero, Seocho-gu, Seoul 06591 (Republic of Korea)
Dr. H. Y. Yoon,[+] Dr. J. H. Park
School of Chemical Engineering, Sungkyunkwan University
2066, Seobu-ro, Jangan-gu, Suwon 16419 (Republic of Korea)
M. K. Shim,[+] Dr. J.-H. Kim
Department of Pharmacy, Graduate School, Kyung Hee University
26, Kyungheedae-ro, Dongdaemun-gu, Seoul 02447 (Republic of Korea)
Dr. S. M. Lee, Dr. S. Lee, Dr. M. G. Pomper
The Russell H. Morgan Department of Radiology and Radiological Science, Johns Hopkins University School of Medicine
601 N. Caroline Street, Baltimore, MD 21287 (USA)
Dr. I. C. Kwon
KU-KIST Graduate School of Converging Science and Technology, Korea University
145 Anam-ro, Seongbuk-gu, Seoul, 02841 (Republic of Korea)
[+] These authors contributed equally to this work.

Supporting information for this article can be found under: http://dx.doi.org/10.1002/anie.201608504.

may also be taken up by normal cells surrounding the tumor tissues, such as fibroblast, muscle, and endothelial cells.[9]

To overcome these drawbacks, we developed a cathepsin B-specific cleavable peptide-substrate caged metabolic precursors that can be specifically cleaved in the cytoplasm of the target tumor cells. This is because cathepsin B is a cysteine protease abundant in the cytoplasm of various tumor cells, such as colorectal cancer,[10] malignant glioma,[11] breast cancer,[12] prostate cancer,[13] and melanoma. Therefore, cathepsin B-specific imaging probes and pro-drugs have received much attention for the development of new theranostic platforms for cancer therapy.[14] The cathepsin B-specific peptide caged metabolic precursor consists of three major components, a cathepsin B-specific cleavable peptide moiety (Lys-Gly-Arg-Arg, KGRR), a spacer linker of *p*-aminobenzyloxycarbonyl (S), and the metabolic precursor of triacetylated *N*-azidoacetyl-D-mannosamine (Ac_3ManNAz), resulting in RR-S-Ac_3ManNAz (Scheme 1 a). We have confirmed that the cathepsin B specifically cleavable peptide moiety of Lys-Gly-Arg-Arg (KGRR) was successfully cleaved by the targeting cathepsin B enzyme using in vitro enzyme tests and in vivo tumor-bearing mice.[15] Importantly, after the cellular uptake of RR-S-Ac_3ManNAz, the dipeptide RR of RR-S-Ac_3ManNAz can be specifically cleaved by cathepsin B in the cytoplasm of cathepsin B-overexpressed tumor cells and then the degraded S-Ac_3ManNAz can be hydrolyzed to produce free Ac_3ManNAz. Finally, free Ac_3ManNAz can generate the chemical receptors on the targeted tumor cells by metabolic glycoengineering and the exogenous chemical receptors can be targeted with bioorthogonal dibenzylcyclooctyne labeled with the near-infrared fluorescent dye Cy5.5 (DBCO-Cy5.5) through click chemistry

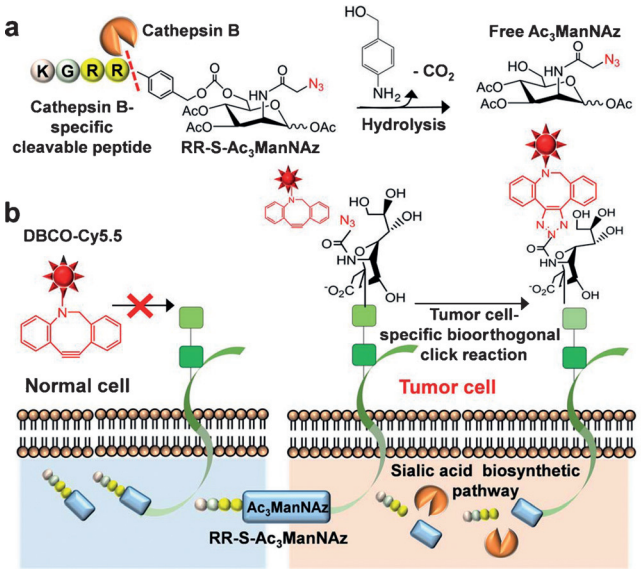

Scheme 1. Schematic of cathepsin B-specific cleavage and fluorescence labeling of metabolic precursor (RR-S-Ac_3ManNAz) in the tumor cell. a) Cathepsin B-specific cleavage of RR-S-Ac_3ManNAz results in the release of a linker, KGRR peptide, and Ac_3ManNAz. b) Tumor-cell-specific bioorthogonal click reaction between exogenous unnatural glycan (chemical receptor) and NIRF-dye-labeled bioorthogonal click molecules (DBCO-Cy5.5).

(Scheme 1 b). Therefore, we expect that the cathepsin B-specific metabolic precursor can produce the chemical receptors on the tumor cell surface in vivo and be used as a new alternative tumor-targeting technique.

To make tumor-cell-targeting metabolic precursor, cathepsin B-specific cleavable metabolite was prepared by chemical conjugation of cathepsin B-specific cleavable peptide (KG*RR*, a recognition site is italicized[16]) with a self-immolative linker (S) to a metabolite (*N*-acetyl azidomannosamine triacetylated), resulting in RR-S-Ac_3ManNAz (Supporting Information, Figure S1). It was purified by reverse-phase high-performance liquid chromatography (RP-HPLC). The molecular weight of RR-S-Ac_3ManNAz was monitored using electrospray ionization mass spectrometry (ESI-MS, *m*/*z* calculated: 1077.1, observed: 1078.1 [M+H^+]) and matrix-assisted laser desorption/ionization analysis (MALDI, *m*/*z* calculated: 1077.1, observed: 1077.5 and 1078.5 [M+H^+]) (Supporting Information, Figure S2). Furthermore, the chemical structure of RR-S-Ac_3ManNAz was analyzed by ^{1}H NMR spectroscopy based on representative characteristic peaks at 1.78 ppm (−CH_3 at acetylated Lys), 1.85–2.0 ppm (−CH_3 at Ac_3ManNAz), and 7.34 and 7.61 ppm (−CH at the PABC linker) (Supporting Information, Figure S3).

Importantly, the degradation of RR-S-Ac_3ManNAz in a cathepsin B solution was clearly observed by HPLC. 3 h post-incubation, the dipeptide RR of RR-S-Ac_3ManNAz started to degrade and was continuously hydrolyzed to give free Ac_3ManNAz, indicating the rapid and successive enzyme reaction (Figure 1 a). Furthermore, free Ac_3ManNAz was gradually cleaved from RR-S-Ac_3ManNAz in a time-dependent manner, indicating the specific enzyme reaction. In the absence of cathepsin B, there was no measurable release of Ac_3ManNAz from RR-S-Ac_3ManNAz in PBS for up to 12 h (Supporting Information, Figure S4). This is because the spacer is very stable when it is linked to both Ac_3ManNAz and RR peptide under physiological conditions.[17] Furthermore, when the RR-S-Ac_3ManNAz was incubated in the presence of cathepsin D, E, L, and caspase-3, we did not observe release of Ac_3ManNAz from RR-S-Ac_3ManNAz for up to 12 h (Figure 1 b). These enzyme assays of RR-S-Ac_3ManNAz in the presence of cathepsin B, D, E, L, and caspase-3 clearly demonstrated the cathepsin B-specific degradation of RR-S-Ac_3ManNAz.

For the tumor-cell-specific generation of chemical receptors by metabolic glycoengineering, the azide groups in the chemical receptors on the tumor-cell surface were directly visualized using DBCO-Cy5.5 in the cell culture system. This is because DBCO has a higher reactivity for the azide groups of unnatural glycans through bioorthogonal click reactions.[18] To confirm the bioorthogonal click reaction on the tumor-cell surface, HT-29 human colon tumor cells were pre-incubated with RR-S-Ac_3ManNAz (5 μM) or Ac_3ManNAz (5 μM) for 24, 48, 72, 96, and 120 h, followed by treatment with DBCO-Cy5.5 (200 nM) for 2 h. Importantly, both RR-S-Ac_3ManNAz- and Ac_3ManNAz-treated HT-29 cells showed the strong NIRF signals on their surfaces, indicating that RR-S-Ac_3ManNAz was successfully cleaved to generate the similar amounts of chemical receptors on the cell surface, compared to free Ac_3ManNAz (Figure 1 c). The relative NIRF inten-

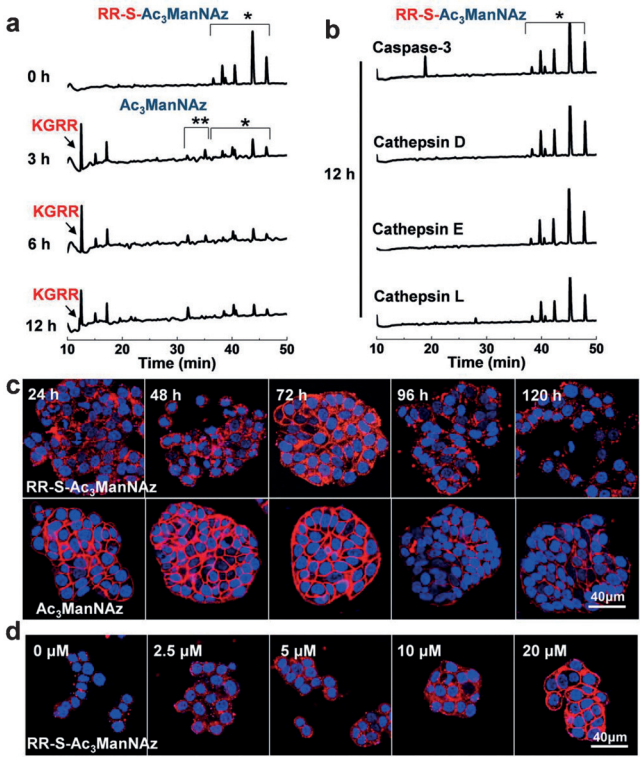

Figure 1. Ac_3ManNAz is released from RR-S-Ac_3ManNAz by cathepsin B, D, E, L, and caspase-3 reaction in vitro. The in vitro release of Ac_3ManNAz was monitored by HPLC at 0, 3, 6, and 12 h for cathepsin B and 12 h for caspase-3, cathepsin D, E, and L as a control experiment. The enzymatic reaction was performed with a) cathepsin B (50 μg mL^{-1}) or b) caspase-3 and cathepsin D, E, and L. * indicates RR-S-Ac_3ManNAz and ** released Ac_3ManNAz. c) Time-dependent confocal microscopy fluorescence imaging of azide groups on the surface of HT-29 cells in vitro. HT-29 cells were treated with RR-S-Ac_3ManNAz (5 μM) or Ac_3ManNAz (5 μM), followed by DBCO-Cy5.5 (200 nM). d) Dose-dependent fluorescence imaging experiments. HT-29 cells were treated with RR-S-Ac_3ManNAz at concentrations between 0 and 25 μM. Red = DBCO-Cy5.5 channel; blue = DAPI channel.

sities of RR-S-Ac_3ManNAz- or Ac_3ManNAz-treated cells at various time points were calculated by measuring the average NIRF intensity of 40 cells in the cell culture system using imaging software ($n = 40$) (Supporting Information, Figure S5). The NIRF intensity of RR-S-Ac_3ManNAz-treated HT-29 cells gradually increased for up to 72 h and decreased 96 h post-incubation. However, free Ac_3ManNAz-treated HT-29 cells showed that the amount of chemical receptors on the tumor cell surface gradually decreased 48 h post-incubation. It is deduced that RR-S-Ac_3ManNAz was gradually cleaved in the cytoplasm of HT-29 cells through the cathepsin B-specific cleavage reaction. Furthermore, RR-S-Ac_3ManNAz can generate chemical receptors on the tumor cell surface in a dose-dependent manner without any cytotoxicity, as shown by increasing the concentration of RR-S-Ac_3ManNAz from 0.1 μM to 20 μM in cell culture media (Figure 1 d and the Supporting Information, Figure S6 a). This means that the amount of chemical receptors was exogenously controlled by delivering different amounts of RR-S-Ac_3ManNAz into the cell culture system. Based on the tumor cell imaging, the concentration of RR-S-Ac_3ManNAz was fixed at 5 μM and the incubation time at 72 h for the expression of chemical receptors on the targeted tumor cell surfaces.

We carefully tested in vitro cathepsin B specificity of RR-S-Ac_3ManNAz as the tumor cell-specific metabolic precursor using an inhibitor of cysteine proteases (Z-FA-FMK) and cathepsin B-suppressed HT-29 cells. First, when the HT-29 cells were pretreated with Z-FA-FMK (50 μg mL^{-1}) for 24 h, RR-S-Ac_3ManNAz-treated tumor cells did not present a strong NIRF signal 2 h post-treatment of DBCO-Cy5.5, compared with tumor cells treated with only RR-S-Ac_3ManNAz. This is because Z-FA-FMK is a very potent irreversible inhibitor of cysteine proteases, including cathepsin B, L, and S, cruzain, and papain.[19] However, free Ac_3ManNAz-treated tumor cells showed a slightly decreased NIRF intensity of DBCO-Cy5.5 in the presence of Z-FA-FMK (Figure 2 a). From this enzyme inhibitor assay, the higher tumor-cell specificity of RR-S-Ac_3ManNAz against the irreversible inhibitor of cysteine proteases was clearly observed. Flow cytometry measurements showed that the mean fluorescence intensities (MFIs) of RR-S-Ac_3ManNAz-treated HT-29 cells were 10-fold higher than those of Z-FA-FMK-treated tumor cells, whereas the NIRF intensities of the Ac_3ManNAz treated groups slightly decreased in the presence of Z-FA-FMK (Figure 2 b). This is because Z-FA-FMK had a negative effect on the proliferation of HT-29 cells in the cell culture system (Supporting Information, Figure S6 b,c).[20] Successful generation of chemical receptors on the surface of HT-29 cells was further analyzed by western blot analysis, in which azide-containing glycoproteins in lysates of HT-29 cells were labeled with phosphine-PEG_3-biotin for 6 h and then separated by molecular weight by 10 % SDS-polyacrylamide gel electrophoresis. The separated glycoproteins were transferred onto PVDF membranes, followed by detection with streptavidin-HRP. Compared with non-treated tumor cells, RR-S-Ac_3ManNAz- and Ac_3ManNAz-treated tumor cells showed strong band intensities of azide-containing sialic acids in the western blot analysis, whereas the azide-containing sialic acids of Z-FA-FMK-treated tumor cells were greatly suppressed, as much as non-treated tumor cells (Figure 2 c). However, the inhibition assay of Z-FA-FMK is not specifically restricted to the targeted cathepsin B in the cell culture system, we further confirmed the cathepsin B-specificity of RR-S-Ac_3ManNAz using cathepsin B-suppressed HT-29 tumor cells.[20] Cathepsin B-suppressed HT-29 cells were prepared by treatment with siRNA complexes consisting of cathepsin B-specific siRNA and lipofectamine 2000. Suppression of cathepsin B in the HT-29 cells was confirmed using western blot analysis (Supporting Information, Figure S8 a), which showed that the azide-containing sialic acids of cathepsin B-suppressed tumor cells were suppressed as much as in non-treated tumor cells (Figure 2 c). Importantly, when cathepsin B-suppressed tumor cells were treated with RR-S-Ac_3ManNAz, they did not present a strong NIRF signal 2 h post-treatment of DBCO-Cy5.5, compared with only RR-S-Ac_3ManNAz-treated wild type tumor cells. However, free Ac_3ManNAz-treated cathepsin B-suppressed tumor cells presented a similar NIRF intensity of DBCO-Cy5.5 to those

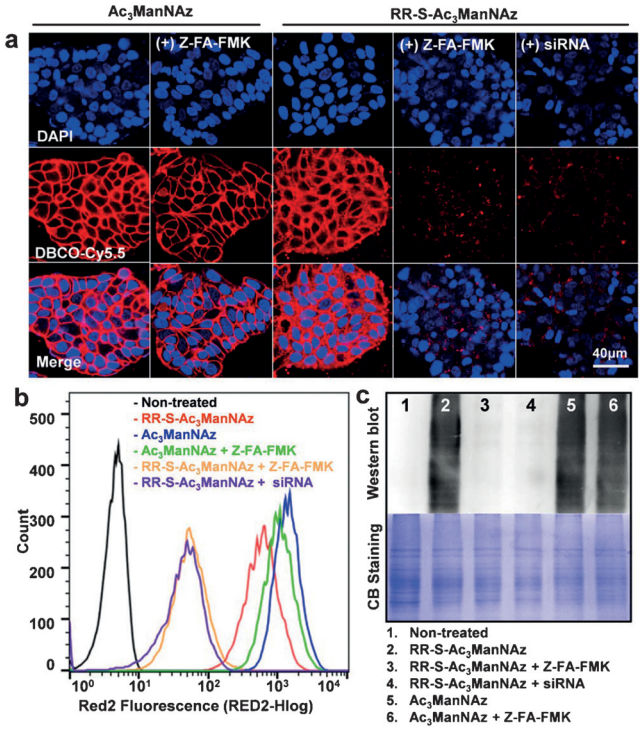

Figure 2. Cathepsin B-specific incorporation of azide as a chemical receptor on wild type HT-29 and cathepsin B-suppressed HT-29 cells. a) Confocal microscopy images of RR-S-Ac_3ManNAz- and Ac_3ManNAz-treated wild type HT-29 and cathepsin B-suppressed HT-29 cells. Azide groups were labeled with DBCO-Cy5.5 for visualization. The HT-29 cells were treated with 50 $\mu g\,mL^{-1}$ of Z-FA-FMK for 24 h before treatment with RR-S-Ac_3ManNAz and Ac_3ManNAz for the inhibition of cathepsin B enzyme activity. The HT-29 cells were treated with 100 nM of Lipo-siRNA(cathepsin B) for 4 h before treatment with RR-S-Ac_3ManNAz and Ac_3ManNAz for suppression of cathepsin B. b) The fluorescence signal was quantified using flow cytometry. c) Western blot analysis of azide groups in glycoproteins in vitro. The coomassie stain shows the total amount of protein.

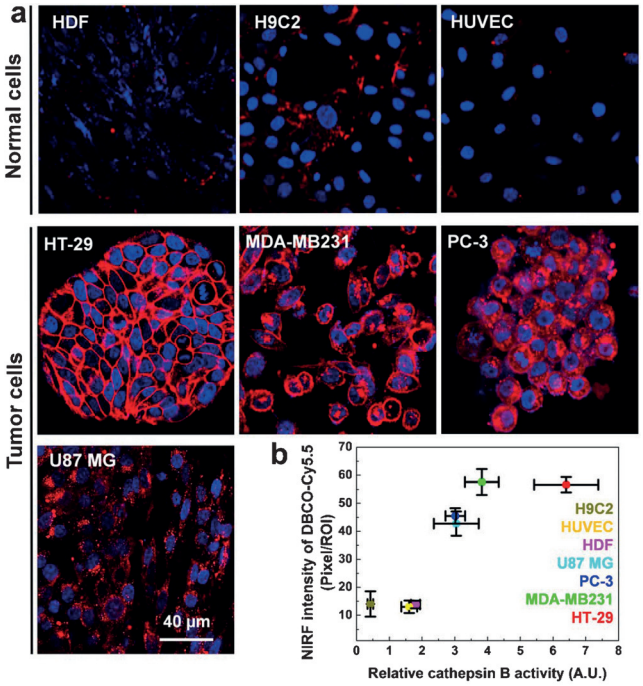

Figure 3. Cathepsin B-specific incorporation of azide groups on HT-29, MDA-MB231, PC-3, and U87 MG tumor cells, compared with normal HDF, H9C2, and HUVEC cells. a) Confocal microscopy images of RR-S-Ac_3ManNAz-treated HT-29, MDA-MB231, PC-3, U87 MG, HDF, H9C2, and HUVEC cells. Azide groups were labeled with DBCO-Cy5.5 for visualization. Red = DBCO-Cy5.5 channel; blue = DAPI channel. b) Quantification of NIRF intensity of confocal microscopy images using ImageJ software and cathepsin B activities from cathepsin B activity assay.

treated wild type tumor cells (Supporting Information, Figure S9a). From the flow cytometry measurements, the MFIs of RR-S-Ac_3ManNAz-treated wild type HT-29 cells were 57-fold higher than those of cathepsin B-suppressed tumor cells, whereas the NIRF intensities of the Ac_3ManNAz-treated groups showed negligible changes of MFIs in both wild type and cathepsin B-suppressed tumor cells (Supporting Information, Figure S9b). This strongly suggests that the cathepsin B-specific RR-S-Ac_3ManNAz must be cleaved by the cathepsin B enzyme that is overexpressed in tumor cells.

The higher specificity of RR-S-Ac_3ManNAz for the cathepsin B enzyme was also tested in different normal and cancer cell lines, such as human dermal fibroblast (HDF), Rat BDIX heart myoblast (H9C2), human umbilical vein endothelial cells (HUVEC), human colon adenocarcinoma (HT-29), human prostate adenocarcinoma (PC-3), human brain glioblastoma (U87 MG), and human breast adenocarcinoma (MDA-MB231) (Figure 3a). First, the cathepsin B expression level of normal cells (HDF, H9C2, and HUVEC) was significantly lower than that of different tumor cells (HT-29, PC-3, U87 MG, and MDA-MB231), which was confirmed using western blot analysis (Supporting Information, Figure S8b,c). Relative band intensity showed that the cathepsin B expression level of tumor cells was 2–200-fold higher than those of normal cells (Supporting Information, Figure S8b). Furthermore, the real degradation of enzyme activity of cathepsin B in normal and tumor cells was carefully quantified using a cathepsin B fluorescence kit. The enzyme activity of cathepsin B in tumor cells is much higher than that of normal cells. In particular, HT-29 cells showed the maximum enzyme intensity of cathepsin B in the cell culture system, compared to that of normal and other cancer cells (Figure 3b). In the cell imaging data, the NIRF intensity of Ac_3ManNAz-treated normal cells and tumor cells presented a similar strong fluorescent intensity after DBCO-Cy5.5 labeling (Supporting Information, Figure S7b). However, RR-S-Ac_3ManNAz-treated normal cells presented the lowest NIRF intensity, owing to the lower level of expressed cathepsin B. Importantly, tumor cells showed strong NIRF intensities that are closely related to the enzyme activity of cathepsin B in tumor cells, which was measured using a cathepsin B fluorescence kit. From these imaging data, the generation of chemical receptors by RR-S-Ac_3ManNAz is strongly correlated with the expression level of cathepsin B in targeted tumor cells. Therefore, we suggest that RR-S-Ac_3ManNAz could generate the chemical receptors by the cathepsin B-specific cleavage mechanism in the cell culture

system, and the exogenously generated chemical receptors could be specifically visualized by labeling with DBCO-Cy5.5 through a bioorthogonal click reaction.

Encouraged by the in vitro tumor cell imaging data, we evaluated the in vivo generation of cathepsin B-specific chemical receptors on the targeted tumor cells by direct tumoral injection of RR-S-Ac_3ManNAz. 1×10^7 HT-29 cells were directly inoculated into both left and right flanks of nude mice ($n=4$). When the tumors grew, RR-S-Ac_3ManNAz was directly injected into the tumor tissue, once a day for four days. As a control experiment, Z-FA-FMK was directly injected into the left tumors four times before injection of RR-S-Ac_3ManNAz for one day. The Z-FA-FMK-treated tumors did not present any side effect on the tumor growth seven days post-injection (Supporting Information, Figure S10a).

One day post-injection of RR-S-Ac_3ManNAz, DBCO-Cy5.5 (4 mg kg^{-1}) was intravenously injected to image the chemical receptors in tumor tissues by in vivo bioorthogonal click chemistry. Interestingly, RR-S-Ac_3ManNAz-treated tumor tissues presented the strongest NIRF intensity in right tumors that were pre-treated with only RR-S-Ac_3ManNAz, whereas Z-FA-FMK-treated left tumors showed a minimum NIRF intensity (Figure 4a). This indicates that RR-S-Ac_3ManNAz successfully generated the chemical receptors on the tumor cell surface in vivo through cathepsin B-specific metabolic glycoengineering. Moreover, ex vivo NIRF images showed that the NIRF intensity of DBCO-Cy5.5 in right tumor tissue was much higher than that of Z-FA-FMK-treated left tumors (Figure 4b). The total NIRF intensity of DBCO-Cy5.5 in the right tumor tissue was 3-fold higher than the left tumor tissue (Figure 4c). The strong NIRF signals of DBCO-Cy5.5 (red) in right tumor tissues were also observed using fluorescence microscopy after immunofluorescence (IF) staining, in which the overexpressed cathepsin B (green) was also clearly observed in both tumor tissues using a FITC-labeled *anti*-cathepsin B antibody (Figure 4d). Western blot analysis clearly showed that the strong azide-containing sialic acid bands were only observed on the RR-S-Ac_3ManNAz-treated right tumors, compared with Z-FA-FMK-treated left tumors (Figure 4e). Finally, we tested our precursor by intravenous injection. When the HT-29 tumor grew, RR-S-Ac^3ManNAz was intravenously injected into tumor-bearing mice, once a day for three days. As control, saline was also intravenously injected into the same tumor models once a day for three days. One day post-injection of RR-S-Ac_3ManNAz, DBCO-Cy5.5 was also intravenously injected into tumor-bearing mice and whole body images were observed one day post-injection. Importantly, the RR-S-Ac_3ManNAz-treated mice presented the higher NIRF signal in the tumor tissues, compared to the saline-treated mice (Supporting Information, Figure S11a). From this, it is deduced that the intravenously injected RR-S-Ac_3ManNAz also can successfully generate chemical receptors on the tumor cell surface in vivo. Moreover, the dissected RR-S-Ac_3ManNAz-treated tumors clearly showed the higher NIRF intensity, compared with the saline-treated tumors (Supporting Information, Figure S11b), as seen in the NIRF average photon counts per gram from excised tumors, which

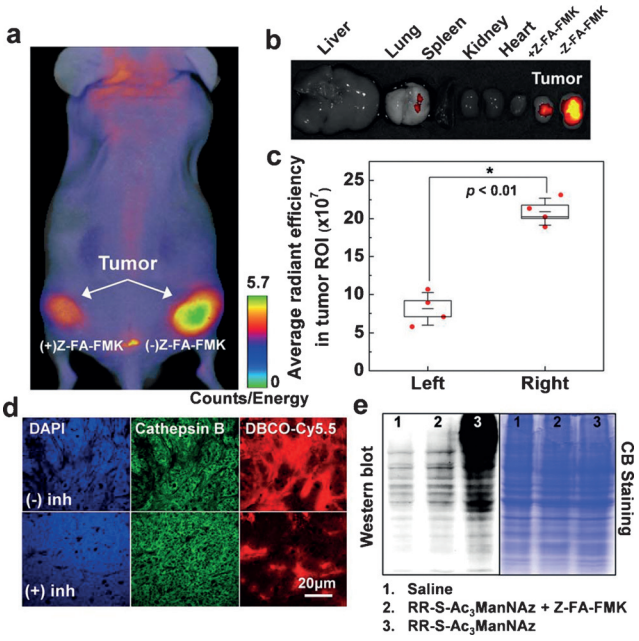

Figure 4. Cathepsin B-specific incorporation of azide groups and labeling of azide groups in HT-29 tumor-bearing mice model ($n=4$) by direct tumoral injection of RR-S-Ac_3ManNAz. For azide incorporation in tumor tissue, 4 mg kg^{-1} of RR-S-Ac_3ManNAz was directly injected into left (Z-FA-FMK (+)) and right (Z-FA-FMK (−)) tumor tissues four times. a) Fluorescence images of azide groups in tumor tissues labeled with DBCO-Cy5.5. b) Ex vivo fluorescence images of major organs and tumors 24 h post-injection of DBCO-Cy5.5. c) Average radiant efficiency in tumor tissues ($n=4$) was quantified using IVIS Spectrum imaging system (PerkinElmer, USA). * indicates difference at the $p<0.01$ significance level. d) Fluorescence images of tumor tissues from (b). Cathepsin B in tumor tissue was visualized by immunofluorescence stain. Red = DBCO-Cy5.5 channel; green = cathepsin B channel. e) Western blot analysis of azide-containing sialic acid in vivo. The coomassie stain shows the total amount of protein.

were 1.7–2-fold higher than that of control saline-treated tumors (Figure S11c).

In conclusion, we have developed a cathepsin B-specific metabolic precursor, RR-S-Ac_3ManNAz, for generating exogenous chemical receptors on the surface of tumor cells. Azide-containing exogenous chemical receptors were successfully generated on HT-29 tumor cells in vitro. Importantly, chemical receptors were also generated in tumor tissues using direct tumoral and intravenously injection of RR-S-Ac_3ManNAz. Subsequently, we can target these chemical receptors using DBCO-Cy5.5 through a bioorthogonal click reaction in vivo. Therefore, our cathepsin B-specific metabolic precursor with bioorthogonal click reaction may be promising for further research in tumor-specific active targeting imaging or drug delivery.

Acknowledgements

This work was supported by the GRL project (NRF-2013K1A1A2A02050115), High Medical Technology Project (HI14C2755) of KHIDI, and the Intramural Research Program (CATS) of KIST.

Keywords: click chemistry · drug delivery · imaging agents · metabolic glycoengineering · tumor targeting

How to cite: *Angew. Chem. Int. Ed.* **2016**, *55*, 14698–14703
Angew. Chem. **2016**, *128*, 14918–14923

[1] J. Du, M. A. Meledeo, Z. Wang, H. S. Khanna, V. D. P. Paruchuri, K. J. Yarema, *Glycobiology* **2009**, *19*, 1382–1401; P. Agarwal, B. J. Beahm, P. Shieh, C. R. Bertozzi, *Angew. Chem. Int. Ed.* **2015**, *54*, 11504–11510; *Angew. Chem.* **2015**, *127*, 11666–11672.
[2] E. Saxon, C. R. Bertozzi, *Science* **2000**, *287*, 2007–2010.
[3] E. M. Sletten, C. R. Bertozzi, *Angew. Chem. Int. Ed.* **2009**, *48*, 6974–6998; *Angew. Chem.* **2009**, *121*, 7108–7133; J. M. Baskin, J. A. Prescher, S. T. Laughlin, N. J. Agard, P. V. Chang, I. A. Miller, A. Lo, J. A. Codelli, C. R. Bertozzi, *Proc. Natl. Acad. Sci. USA* **2007**, *104*, 16793–16797.
[4] E. Ruoslahti, S. N. Bhatia, M. J. Sailor, *J. Cell Biol.* **2010**, *188*, 759–768.
[5] A. Schroeder, D. A. Heller, M. M. Winslow, J. E. Dahlman, G. W. Pratt, R. Langer, T. Jacks, D. G. Anderson, *Nat. Rev. Cancer* **2012**, *12*, 39–50.
[6] H. Koo, S. Lee, J. H. Na, S. H. Kim, S. K. Hahn, K. Choi, I. C. Kwon, S. Y. Jeong, K. Kim, *Angew. Chem. Int. Ed.* **2012**, *51*, 11836–11840; *Angew. Chem.* **2012**, *124*, 12006–12010; S. Lee, H. Koo, J. H. Na, S. J. Han, H. S. Min, S. J. Lee, S. H. Kim, S. H. Yun, S. Y. Jeong, I. C. Kwon, K. Choi, K. Kim, *ACS Nano* **2014**, *8*, 2048–2063.
[7] L. Dafik, M. O'Alarcao, K. Kumar, *Bioorg. Med. Chem. Lett.* **2008**, *18*, 5945–5947.
[8] P. V. Chang, D. H. Dube, E. M. Sletten, C. R. Bertozzi, *J. Am. Chem. Soc.* **2010**, *132*, 9516–9518.
[9] C. Sävblom, J. Malm, A. Giwercman, J.-Å. Nilsson, G. Berglund, H. Lilja, *Prostate* **2005**, *65*, 66–72.
[10] K. Hirai, M. Yokoyama, G. Asano, S. Tanaka, *Hum. Pathol.* **1999**, *30*, 680–686; E. Campo, J. Muñoz, R. Miquel, A. Palacín, A. Cardesa, B. F. Sloane, M. R. Emmert-Buck, *Am. J. Pathol.* **1994**, *145*, 301–309.
[11] S. A. Rempel, M. L. Rosenblum, T. Mikkelsen, P.-S. Yan, K. D. Ellis, W. A. Golembieski, M. Sameni, J. Rozhin, G. Ziegler, B. F. Sloane, *Cancer Res.* **1994**, *54*, 6027–6031.
[12] M. Sameni, E. Elliott, G. Ziegler, P. H. Fortgens, C. Dennison, B. F. Sloane, *Pathol. Oncol. Res.* **1995**, *1*, 43–53.
[13] A. M. Szpaderska, A. Frankfater, *Cancer Res.* **2001**, *61*, 3493–3500.
[14] T. Fujii, M. Kamiya, Y. Urano, *Bioconjugate Chem.* **2014**, *25*, 1838–1846; P. Habibollahi, J.-L. Figueiredo, P. Heidari, A. M. Dulak, Y. Imamura, A. J. Bass, S. Ogino, A. T. Chan, U. Mahmood, *Theranostics* **2012**, *2*, 227–234; J. Tian, L. Ding, Q. Wang, Y. Hu, L. Jia, J.-S. Yu, H. Ju, *Anal. Chem.* **2015**, *87*, 3841–3848; L. H. Shao, S. P. Liu, J. X. Hou, Y. H. Zhang, C. W. Peng, Y. J. Zhong, X. Liu, X. L. Liu, Y. P. Hong, R. A. Firestone, *Cancer* **2012**, *118*, 2986–2996; X. Zhang, K. Tang, H. Wang, Y. Liu, B. Bao, Y. Fang, X. Zhang, W. Lu, *Bioconjugate Chem.* **2016**, *27*, 1267–1275; Y.-J. Zhong, L.-H. Shao, Y. Li, *Int. J. Oncol.* **2013**, *42*, 373–383; C. S. Gondi, J. S. Rao, *Expert Opin. Ther. Targets* **2013**, *17*, 281–291.
[15] J. Hee Ryu, S. Ah Kim, H. Koo, J. Young Yhee, A. Lee, J. Hee Na, I. Youn, I. Chan Kwon, B.-S. Kim, K. Kim, *J. Mater. Chem.* **2011**, *21*, 17631–17634; J. H. Ryu, J. H. Na, H. K. Ko, D. G. You, S. Park, E. Jun, H. J. Yeom, D. H. Seo, J. H. Park, S. Y. Jeong, *Biomaterials* **2014**, *35*, 2302–2311.
[16] R. A. Maciewicz, D. J. Etherington, *Biochem. J.* **1988**, *256*, 433–440.
[17] M. Dorywalska, P. Strop, J. A. Melton-Witt, A. Hasa-Moreno, S. E. Farias, M. Galindo Casas, K. Delaria, V. Lui, K. Poulsen, C. Loo, S. Krimm, G. Bolton, L. Moine, R. Dushin, T.-T. Tran, S.-H. Liu, M. Rickert, D. Foletti, D. L. Shelton, J. Pons, A. Rajpal, *Bioconjugate Chem.* **2015**, *26*, 650–659.
[18] C. P. Ramil, Q. Lin, *Chem. Commun.* **2013**, *49*, 11007–11022.
[19] T. Rajah, S. C. Chow, *PloS one* **2015**, *10*, e0123711.
[20] F. J. Lopez-Hernandez, M. A. Ortiz, Y. Bayon, F. J. Piedrafita, *Mol. Cancer Ther.* **2003**, *2*, 255–263.

Received: August 31, 2016
Published online: October 20, 2016

